EUROPEAN ORGANIZATION FOR NUCLEAR RESEARCH

CERN-EP/83-166
24 October 1983

A HIGH-RESOLUTION SPECTROMETER FOR THE STUDY OF HIGH-MASS MUON PAIRS PRODUCED BY INTENSE HADRON BEAMS

NA10 Collaboration

CERN[1]–Naples (Univ. and INFN)[2]–Palaiseau (Ecole Polytechnique)[3]–
Strasbourg (CRN and Univ. Louis-Pasteur)[4]–Zurich (ETH)[5]

L. Anderson[3,a)], R. Benetta[1)], J.D. Berst[4)], B. Betev[1,b)], J.J. Blaising[4)],
P. Bordalo[3)], A. Boumediene[3)], L. Cerrito[3)], A. Coc[3,c)], A. Degré[4)],
Ph. Delcros[3)], A. Ereditato[4,d)], S. Falciano[5,e)], K. Freudenreich[1)],
J.P. Froberger[1)], J.C. Gouache[1)], C. Gregory[3)], A. Gsponer[5,f)],
M. Guanziroli[5)], P. Gudewicz[4,g)], H. Hofer[5)], P. Juillot[4)], P. Klein[4)],
L. Kluberg[3)], A. Lacourt[1)], P. Lecomte[5)], J. Lecoq[4)], P. Le Coultre[5)],
R. Morand[4)], M. Morpurgo[1)], B. Mours[4)], J.Y. Parey[3)], G. Remy[4)], A. Romana[3)],
R. Salmeron[3)], P. Strolin[2)], H. Suter[5)], G.J. Tarnopolsky[5,h)], V.L. Telegdi[5)],
J. Varela[3,i)], G. Viertel[5)], J. Wallace-Hadrill[1,j)] and M. Winter[4)]

ABSTRACT

We describe the design, construction and performance of a high-resolution spectrometer used at CERN to study the production of high-mass muon pairs by intense hadron beams. We also discuss the on- and off-line software used with this spectrometer.

(Submitted to Nuclear Instruments and Methods in Physics Research)

---

a) Present address: Sunny Vale, California, USA.
b) Permanent address: Institute for Nuclear Research and Nuclear Energy, Sofia, Bulgaria.
c) Now at Laboratoire René Bernas, Université de Paris XI, Orsay, France.
d) Now at University of Naples and INFN, Naples, Italy.
e) Now at INFN, Sezione di Roma, Italy.
f) Now at GIPRI, Geneva, Switzerland.
g) Now at CEA, Valduc, France.
h) Now at SLAC, California, USA.
i) Now at Centro di Fisica da Materia Condensada, Lisbon, Portugal.
j) Present address: Reynolds Farm, Cassington, Oxford, England.

1. INTRODUCTION

The spectrometer described here was designed to measure, with high statistics and good mass resolution, the production of high-mass muon pairs by pions [1]. As the cross-section for such a process is very low (a few picobarns for masses above 10 GeV/c^2), special attention was devoted to the optimization of parameters governing luminosity and sensitivity, keeping a good mass resolution.

High luminosity is provided by a very intense beam (up to 2×10^9 π^- per burst at 200 GeV/c), a heavy nuclear target (12 cm of tungsten), and a large acceptance spectrometer which measures and identifies the muons (fig. 1). Correspondingly, the detectors were designed to stand efficiently high rates [10 MHz for the counters and 100 kHz for each wire of the multiwire proportional chambers (MWPCs)], and to allow for a good mass resolution (20%) at the trigger level.

The trigger is formed with signals from two sets of two hodoscopes, one set located upstream (R1 and R2) and the other downstream (R3 and R4) of a spectrometer magnet. Their geometry and granularity were chosen to allow fast and selective triggering on muons pointing at the target and having transverse momenta in a specified range.

The measurement of the trajectories of the muons before and after deflection by the azimuthal magnetic field is performed with two corresponding sets of four MWPCs. The final mass resolution (3 to 4%) is determined by the accuracy with which angles and momenta are measured, and is limited by multiple scattering and energy loss straggling in the hadron absorber and by the uncertainty of vertex localization.

2. BEAM LINE AND MONITORING

2.1 Hadron beam

The spectrometer is located in the CERN North Area High-Intensity Facility [2] at the end of a high-intensity hadron beam. This beam line can transport primary protons and negative secondaries of up to 450 GeV/c, and positive secondaries of up to 300 GeV/c. Despite its large momentum bite of $\pm 10\%$ it has only a spot size of about 0.5 cm FWHM at its focus, i.e. our target.

The beam line is relatively short (190 m) and has two weak horizontal bends (11 mrad each). Therefore, in addition to the muons from the beam pion decays, the spectrometer is exposed to muons from the decays of off-momentum secondaries within the first 40 m, and to muons originating from the proton beam dump 60 m downstream of the production target. About 22 m of magnetized iron scrapers are installed in order to reduce this muon halo. Moreover, the apparatus itself is made insensitive to halo muons in the central beam region and on one side in the horizontal bending plane. The hottest counter of the spectrometer sees approximately 10^{-2} particles per square metre and per incident π, a fact which agrees with the predictions of a simulation program (HALO [3]).

A beam of 5×10^{12} protons of 400 GeV/c hitting the production target yields 1.9×10^9 negative secondaries (95% π^-, 4.4% K^-, and 0.6% $\bar{p}$) of 200 GeV/c [4], and 2.7×10^8 (98.8% π^-, 1.15% K^-, and 0.05% $\bar{p}$) of 300 GeV/c [4]. With protons of 450 GeV/c the yield is expected to rise to 3.1×10^9 at 200 GeV/c, and to 7.8×10^8 at 300 GeV/c.

2.2 Monitoring

The incident flux is monitored with two independent multifoil ionization chambers filled with argon [5], and with several scintillation telescopes pointing at 90° at the target. The linearity and absolute calibration of these monitors were determined at low intensity with reference to a scintillation counter inserted into the beam line. A better and more convenient calibration is obtained by activating stacks of carbon foils at the target location at full intensity; this also provides true beam profiles. The position and profile of the beam are also continuously monitored with two wire ionization chambers.

The momentum distribution of the beam is determined by measuring the transmitted flux as a function of the position of a slit in the plane of maximum momentum dispersion.

3. SPECTROMETER

One goal of the experiment is to investigate scaling invariance as a function of energy; this is best done if the spectrometer acceptance is made independent of the energy. For an axially symmetric spectrometer this is achieved if the positions of the various components are expanded along the spectrometer axis as $\sqrt{(s/s_0)}$ when going from a centre-of-mass energy $\sqrt{s_0}$ to a centre-of-mass energy $\sqrt{s}$. The target, the hadron absorber, and the first hodoscope (R1) being fixed, the acceptance is kept independent of energy by displacing the other components in that ratio.

3.1 Target

The acceptance of the trigger is optimized for a point located 40 cm upstream of the hadron absorber.

Three targets, together with an empty target holder, are mounted symmetrically on a remote-controlled wheel. The targets are embedded in a Rohacell cylinder, 5 cm in diameter. Data were taken mainly with a tungsten target (12 cm long and 1.8 cm in diameter; density 18.26 g/cm^3).

3.2 Hadron absorber

The hadron absorber consists of the following parts:

i) A conical tungsten/uranium core, serving as the main beam dump. In order to achieve, already at the trigger level, a good separation of the dimuons produced in the target from the background originating in the beam dump, the latter starts 120 cm downstream of the target.

ii) A toroidal muon filter, covering the angular acceptance of the spectrometer and starting 40 cm downstream of the target. It consists of seven graphite disks, each 40 cm thick and of increasing diameter, followed by four similar iron disks, and again a graphite disk, for a total of 480 cm. Owing to the target constraint and to the short lever arm to the spectrometer, the multiple scattering in the iron disks affects the dimuon mass resolution only mildly.

iii) An iron and concrete shielding wall, encasing the toroidal absorber.

3.3 Toroidal spectrometer magnet

This magnet has hexagonal symmetry. An essentially azimuthal field $B = B_\phi(r)$ is excited between six laminated, wedge-shaped, iron pole pieces, each subtending 18° in azimuth. The air-core part of the magnet, consisting of sectors between the iron wedges, thus subtends 70% of the azimuthal acceptance. The windings (see fig. 1) are assembled into six coils converging radially to the axis of the magnet.

Over almost the entire air-core volume, the field has the designed dependence $B_\phi = B_0/r$ with a high degree of homogeneity. The 1/r-dependence of the field is particularly useful for the magnetic analysis of particles exiting from a target on the magnet axis. To an excellent approximation, one has for the deflection angle universally:

$$\theta = (p_0/p_T) \times \ln(z_2/z_1),$$

where p_0 = 6.08 GeV/c = magnet constant; p_T = particle transverse momentum; z_1, z_2 = distances of the effective entrance and exit planes of the magnet from the target.

The main geometrical and electrical parameters of the magnet are given in table 1.

At a mean radius r = 75 cm, B_ϕ = 0.728 T with an exciting current of 10000 A, and $\int B_\phi \, d\ell$ = 2.9 T·m. Up to r = 95 cm, the homogeneity is 0.1%. For reasons of cooling and to economize on energy, the magnet is pulsed during each burst. The polarity can be reversed on a burst-by-burst basis. The field is continuously monitored (see subsection 5.2.4.5). Although the field map was established in d.c. regime at reduced current, it was verified that it agreed with the field map in the pulsed operation. This map was parametrized analytically using polynomial and spline functions.

3.4 Hodoscopes

3.4.1 R hodoscopes

The R-hodoscope design (fig. 1) is adapted to the sixfold symmetry of the spectrometer magnet. Each radial hodoscope R1 to R4 thus consists of six sextants, each covering 60° in azimuth, except for two sextants in R3 and R4 which, being the ones most exposed to the halo of the pion beam, were reduced to 46°. There are 32 counters per sextant in R1, R2, and R4, and 24 in R3, giving a total of 720 channels.

For a given sextant, the knowledge of the counters hit by a particle in each hodoscope provides a rough measurement of its trajectory before and after deflection by the magnetic field. Hodoscopes R1 and R2 measure the production angle and, in conjunction with R3 and R4, determine the transverse momentum. For a given location of the hodoscopes along the spectrometer axis, the radial widths of the counters define, for the purposes of the trigger, the spatial resolution at the target and in transverse momentum.

Simple geometrical arguments show that the widths of successive counters of both R1 and R2 must form a geometrical progression, i.e. $w_n = w_1 \times \rho^n$, so that each corresponding n^{th} pair of counters in these hodoscopes can view the same axial interval about the target.

As the expected counting rate limits the size of the most exposed counters, and given the fact that R2 covers the fixed entrance aperture of the magnet, the choice of 32 elements per sextant and of 12.3 mm for the width of the innermost counter of R2 gives ρ = 1.043. The ratio of the widths of the corresponding counters must equal that of the distances of R1 and R2 from the target centre, and determines the acceptance of the spectrometer. For the 250 GeV/c set-up this ratio was chosen as ρ^6.

The counters of R3 and R4 all have the same width (5.5 cm), chosen to give 0.3 GeV/c resolution in the transverse momentum p_T, for muons with $p_T < 1.5$ GeV/c.

3.4.2 P hodoscopes

Two hodoscopes, P1 and P2 (fig. 1), one on each side of the magnet, are mounted to impose further constraints on the trajectories defined by the trigger. Hodoscope P1 is made of 48 triangular counters, each subtending 7.5° in azimuth; P2 also consists of 48 counters scaled to the P1 counters with a slight increase to allow for the multiple scattering in the hadron absorber.

These hodoscopes have only been used to define a test trigger on halo particles, or to provide a special trigger to determine the efficiency of the standard trigger (see subsection 4.4.4).

3.4.3 Scintillation counters

The electronics associated with the counters was designed to stand 10 MHz. As the anode current of photomultipliers is generally limited to 200 μA, it is necessary to operate them at very low gain. This constraint is particularly critical when the signals have to be transmitted over 50 m before discrimination and shaping. Another constraint is given by the big variations is pulse height over scintillator length (up to 2.4 m), which induce a corresponding time jitter after discrimination. On these grounds, we made the following choices:

i) The scintillator material is NE110*), 1 cm thick, wrapped in aluminium foil, and viewed by simple fishtail-shaped light-guides; the guides are kept short to minimize Cherenkov pulses and hence the current drawn by the photomultiplier.

ii) The gain of the photomultipliers (Philips 1982, 12-stage) is unaffected by flux variations from 10^4 to 10^7 Hz; the dark current at high flux is below 20 nA.

iii) The voltage divider is optimized to stabilize the gain at high rate; the last three dynodes are supplied with boosters to avoid saturation of the anode current.

iv) The signals are shaped at the photomultiplier outputs with 2 ns long cables terminated with 9 Ω to attenuate the overshoots.

v) A fast amplifier (gain 10) processes the signal before transmission through a 50 m long coaxial cable (RG213).

vi) The signals are discriminated in the counting room at 15 mV with updating discriminators designed for 200 MHz.

Tests showed that even the largest counter (240 × 5 cm^2) was 99.5% efficient over its full length at 10 MHz.

During data-taking periods, the efficiency of the hodoscopes R1, R2, R3, and R4 is monitored with special triggers. Analysis of these proved that the hodoscopes had always efficiencies above 99%.

3.5 Multiwire proportional chambers

3.5.1 Chamber design

The MWPCs form two groups of four: the large chambers downstream of the magnet and the small ones upstream of it; their construction closely followed a CEN Saclay design.

Each of the eight hexagonally shaped MWPCs (figs. 2a and 2b) consists of three independent planes, each with two graphited Mylar cathodes and one anode wire plane. Each wire plane is rotated by 60° relative to the other two (y, u, v coordinates, altogether 24 planes). The gap between the

---

*) Nuclear Enterprises Ltd., Scotland, UK.

cathode and the wire plane is 0.6 cm, and the separation between the 20 μm gold-plated tungsten wires is 0.3 cm. The small chambers have 749 wires per plane, the large ones 1229; three (respectively five) Kapton spacers with a field-correcting wire are mounted to support the wires.

3.5.2 Chamber operation

A gas mixture of argon (80%) + isobutane (19.8%) + freon (0.2%) is used. Half of the argon is flushed through isopropylic alcohol at 4 °C. An on-line gas analyser monitors the operation of the mixing station continuously. In operation, the flow is half a chamber volume per day.

The chambers operate at a nominal voltage of 2800 V, lowered to 2400 V between bursts. Because of the intense muon halo near the centre and on one side of the beam line, a keyhole-shaped region (fig. 2a) of the chambers is made insensitive by keeping a corresponding region of the cathode (insulated from the rest of it by a 3 mm gap) at 2200 V. A plateau curve is shown in fig. 3a; the dotted line shows the corresponding dark current. Currents up to 2.5 mA per gap were recorded during bursts, depending on the beam momentum and intensity.

In three years of operation (corresponding to about three months of effective running), no deterioration of the chamber performance was seen. This agrees with preliminary tests with X-rays and a 60 Ci ^{192}Ir source, which we performed to simulate the ageing processes. We observed a 20% decrease of the pulse height after 24 hours of illlumination, operating at 11 mA.

3.5.3 Chamber performance and readout

We observed counting rates of up to 200 kHz per wire. Figure 4 shows the chamber efficiency as a function of beam intensity. Curve (a) is the expected efficiency drop in one gap assuming a dead-time of 200 ns (signal length) and allowing for the observed chamber illumination. Curve (b) is the efficiency calculated from on-line reconstructed tracks (see subsection 5.2.4.2). Curve (c) is a "local efficiency" measurement made with a small scintillator telescope. Using off-line reconstructed tracks, we determined that the chamber inefficiency is constant along the wires, and varies from about 2 to 4% from the edges to the centres of the chambers.

In the actual working conditions, the chamber pulses are typically 200 ns long and have amplitudes of 30 $\pm$ 6 mV at the output of the preamplifier cards. At the wire end opposite the preamplifier input, a Lecher-line is provided in order to inject test pulses. On each amplifier card (4237 RMH [6]) 32 channels are equipped with a preamplifier (500 Ω input impedance), a differential amplifier with a gain of 7 $\pm$ 1, and a driver. The 2 $\times$ 32 differential output signals are fed through 120 m long twisted-pair delay-line cables — attenuating the signal by a factor of 2 — to the pattern units (4236 RMH [6]) in the counting room. There they are discriminated at 8 mV and strobed by 100 ns wide (fig. 3b) trigger signals.

4. TRIGGER LOGIC

4.1 Trigger principle

Events of interest are high-mass muon pairs and multimuon events produced in the target. Except for punch-throughs, the hadron absorber behind the target transmits only muons. These include

- prompt muons produced in the target or in the absorber itself;
- muons travelling along the beam line (halo);
- muons from pions and kaons produced in the target and decaying before being absorbed.

The punch-throughs are that small fraction of hadrons which emerge from the absorber, frequently as a high-multiplicity shower of low-energy particles.

Given these facts, trigger selectivity for a single particle is achieved in the following way:

i) By favouring tracks originating in the target, both against those produced in the absorber and those travelling parallel to the beam (halo muons). The geometry of the hodoscopes R1 and R2 was chosen with this goal in mind (see subsection 3.4.1). The associated fast logic selects particles produced in the target. The position of the counters hit (V = R1·R2 coincidence) defines the production angle.

ii) By providing a rough measurement of the transverse momentum p_T. The R4 hodoscope downstream of the magnet yields p_T in conjunction with R1 and R2.

iii) By constraining the V·R4 coincidence with the hodoscope R3. This reduces the rate of accidental coincidences between uncorrelated tracks before and behind the magnet.

These simple geometrical criteria are implemented with fast electronics for muons traversing the corresponding sextants of R1, R2, R3, and R4. There are thus six identical logic circuits, each one imposing the above requirements.

The *first-level trigger* is obtained by requiring at least one particle simultaneously in two different sextants. Combining the p_T measurements, a rough cut can be imposed on the dimuon mass already at this level.

These constraints are very effective on low-multiplicity events. However, some showers emerging from the absorber may fire a large number of channels, thereby destroying the trigger selectivity. A *second-level trigger,* based on an event-buffer/microprocessor system, restores and even improves this selectivity by rejecting high-multiplicity events and, in addition, performs a more refined mass calculation.

4.2 Fast logic

Each counter signal is discriminated at 15 mV and shaped to ECL level. Each sextant is processed in two 16-channel modules*) linked with twisted-pair cables (fig. 5).

As already mentioned, the logic is a sixfold system, each subsystem dealing with the signals from one sextant, as described below.

A first stage forms the coincidence V = R1·R2. A second stage, performed in an ECL matrix [7], forms the required threefold coincidences V·R3·R4 out of the 32 × 24 × 32 possibilities. They correspond to 1024 p_T values, determined by the V·R4 combinations involved. This matrix provides the inputs for the first and second trigger levels as follows:

- The 1024 V·R4 coincidences are OR-ed to form four signals (A, B, C, and D) chosen to define four rough p_T bins, limited by 4, 2, 1.4, and 0.6 GeV/c. As mentioned, the first-level trigger combines these signals from different sextants to give an estimate of the dimuon mass.
- These 1024 V·R4 coincidences are also strobed by the first-level trigger into the memory of the hard-wired p_T processor of the second-level trigger. If several p_T's are fired in one sextant, a priority encoder selects the highest one for each V. Then in 15 μs the p_T processor selects the highest p_T amongst all occurring V·R4 coincidences.

---

*) LeCroy Research Systems SA, Geneva, Switzerland.

4.3 First-level trigger

The 6 × 4 signals (A, B, C, D) from the sextants are fed to a logic unit. This unit, built in CAMAC, may be programmed to select any combination of sextant pairs specified by their p_T bins A, B, C, and D: there are 15 combinations of sextant pairs and 10 combinations of A, B, C, and D for each sextant pair.

The limits of the p_T bins are chosen in such a way as to cut low-p_T muons ($p_T < 0.6$ GeV/c), and to tag dimuons below the J/ψ (DD combination), within the J/ψ region (CD, BD, and CC), and above the J/ψ. The hardware allows an easy modification of these bins.

If more than two sextants are hit, a priority encoder selects the combination corresponding to the highest mass (this lowers the trigger rejection but maintains its efficiency).

The first-level trigger strobes the full event information into RMH memory modules: counter hits in the hodoscopes, wire hits in the chambers, and associations performed by the fast logic, i.e. V coincidences; A, B, C, and D measured in each sextant; sextant pairs associated with the logic unit. The RMH modules connected to the fast logic were modified to accept ECL levels.

Depending on the pulse structure and intensity of the beam, the first-level trigger rate may rise as high as 600 per burst. This rate is reduced by a second-level trigger based on a microprocessor acting after an event has been stored in its fast buffer memory (150 ns cycle time) and before its transfer (3 μs cycle time) to the ND 100/500 computer memory (see subsection 5.2.2).

4.4 Second-level trigger

4.4.1 Description

The second-level trigger consists of a fourfold event-buffer/microprocessor system as shown in fig. 6. Each buffer is a 4 Kbyte multiport memory (CMOS static RAM, 150 ns access time) connected to the RMH readout system, to the computer via CAMAC, and to a special-purpose microprogrammable bit-slice microprocessor "GESPRO" [8]. Each microprocessor is directly connected to the fast logic through the six hard-wired p_T processors.

Upon arrival of a first-level trigger, a controller assigns an available buffer and initiates the transfer of data from the RMH system into the corresponding memory. At the same time, reading the information in the p_T processor, GESPRO starts computing the dimuon mass according to the formula:

$$M^2 = 2p_1p_2\,[1 - \cos\theta_1 \cos\theta_2 - \sin\theta_1 \sin\theta_2 \cos(\phi_1 - \phi_2)]\,,$$

where p_i, θ_i, and ϕ_i, are the momenta and angles defined respectively by V·R3·R4, V, and the sextant hit.

This calculation, performed in less than 13 μs, is finished *before* transfer from the RMH memory to the buffer memory. If the mass is below a given value, the readout may be aborted and the system reinitialized. If, during readout, the number of words associated with the event exceeds a programmable value, it may also be aborted.

Upon completion of the transfer to the buffer memory, GESPRO starts the other computations relevant to the cuts requested. The cuts implemented so far and which may lead to the rejection of an event are the following:

- total number of words in the event;
- total number of counters hit in R1, R2, R3, and R4;
- mass of the dimuon smaller than a given value (e.g. < 2 GeV/c^2) or lying within a mass bin (the number of J/ψ's retained may be prescaled);
- alignment of the counters V · R3 · R4 (refining the selection made by the ECL matrix where some misaligned combinations were tolerated to simplify the hardware);
- validation of the event by hodoscopes P1 and P2.

In addition, GESPRO tags the multimuon candidates.

4.4.2 Performance

The sequence of cuts was defined considering the rejection and processing time of each one. Table 2 shows this sequence with the average performance of each selection.

These cuts provided a total rejection factor of between 4 and 10 depending on pion intensity (1 to 2×10^9 π/burst). The inefficiencies introduced by the second-level trigger never exceeded 2%. They are permanently monitored by allowing a small sample of first-level triggers to pass all the cuts, the rejections being flagged. As these cuts are effective after RMH readout and before transfer to the ND 100/500 via CAMAC, the second-level trigger reduces not only the volume of data written on tape but also the experimental dead-time.

At 10^9 π per burst, 70% of the triggers were found to be good events, compared to 40% at 2×10^9 π per burst.

4.4.3 Setting-up of the hodoscopes and of the fast electronics

With very high rates, it is of prime importance to time the counters perfectly in order to sharpen the time resolution of the logic combinations. At an incident rate of over 10^9 particles per second, it is not possible to provide a synchronization signal from a beam-tagging counter. Therefore each sextant of R2 and R3 was provided with a timing counter (T), running along its bisector across all of its counters. Each T counter is viewed at both ends by photomultipliers whose signals are fed to a mean-timer. Having first synchronized the different T counters, it becomes easy to time in, with good accuracy (< 0.5 ns), all the R counters. With such a timing, the widths of the fast logic signals are mainly defined by the time jitter due to the distribution of the particle hits along each scintillator (R1: 8 ns; R2: 4 ns; V: 12 ns; R3: 20 ns; R4: 20 ns; A, B, C, D: 25 ns). As the coincidence circuits work in a linear mode, accurate timing of all logic combinations was achieved by using R2 as a reference. The T counters are also used to measure and monitor the R counters' pulse heights.

Since all the discriminators have a test input which can be activated in any channel via CAMAC, a test program was implemented to perform

- the selection of any pattern of R1, R2, R3, and R4, and the check of the operation of any logic combination whose result is read in the RMH memory system;
- the delay curves on any combination of V or of V · R3 · R4, thus testing the ECL matrix in detail;
- the delay curves between p_T's measured in different sextants, thus testing the first-level trigger unit;
- the delay curves for the latch of the event information into the RMH memory system.

With these pulser signals, the fast logic was timed to better than 1 ns, the limit being set by the time dispersion between channels in the same logic module.

4.4.4 Monitoring of the trigger efficiency

A special trigger is implemented for off-line monitoring of the efficiency of the standard trigger; using hodoscopes P1 and P2, two particles are selected in different sextants. The trigger is further constrained, requiring

- that the standard first-level trigger finds at least one particle with $p_T > 0.6$ GeV/c;
- that the microprocessor detects a low-multiplicity event (in terms of wire hits) with two track segments pointing at the target.

Thus one triggers on dimuons using the standard trigger for *one* muon, leaving the other muon unbiased.

5. ON-LINE PROCESSING

5.1 Design considerations

We recall the main features of the experiment, which guided the design of the on-line system:

- the repetition rate of the Super Proton Synchrotron (SPS) is 10 to 12 s, with a spill duration of 1 to 2 s;
- even at high trigger rates, the acquisition dead-time should be kept at a minimum;
- there is a large number of readout channels: 19968 for the MWPCs, 816 for the counters, and 320 for the trigger logic;
- a maximum of monitoring should be performed in real time, so that failures of the apparatus and/or of the beam line can be detected promptly.

5.2 Description of the on-line system

5.2.1 Readout

As already mentioned in previous sections, we have adopted the RMH system [6]. A total of 660 receiver modules are housed in 34 crates, grouped into 9 branches, one branch for each chamber and one for the hodoscopes and the trigger logic. A system encoder accesses the nine branches through nine branch receivers. The data from the system encoder are then transferred to one of the four event-buffers (see subsection 4.4.1) through fan-outs (one per buffer).

An event is fully specified by the addresses of the wire hits, by the pattern of the hodoscopes, and by the result of logic operations. In order to pass all the information through the fast RMH readout, thus optimizing the data flow, no analog information (pulse shapes, time spectra, etc.) is transmitted.

5.2.2 Data-acquisition program

The on-line computer is a Norsk Data ND 100/500 system, with 2 Mbytes of memory, two 1600-bpi magnetic tape drives, and a 75 Mbyte disk. The ND 500 is a fast, byte-addressable processor which needs a front-end processor for the I/O functions. These are performed by the ND 100, a 16-bit computer with real-time programming facilities. Both processors share the 2 Mbyte multi-port memory.

In order to reduce the dead-time due to the handling of external interrupts, the data acquisition is not triggered event-by-event; at beginning-of-burst (BOB) the CAMAC direct memory access (DMA) channel is initialized to accept data from the event-buffer system. The data are then directly stored into a 364 Kbyte burst-buffer in the multi-port memory. The DMA interface cannot address

364 Kbytes; therefore, blocks of 32 Kbytes are transferred. After the end of a transfer, a look-at-me (LAM) is generated and the program initializes the interface for the next block.

Data-taking is interrupted either when the burst-buffer is full or when the interrupt for the end-of-burst (EOB) is received. At EOB the auxiliary information (scalers, magnet current, beam status, etc.) is read in via CAMAC, and the processing in the ND 500 is activated, with the following tasks:

- decoding of the burst-buffer to find the events (marked by special flags);
- tape formating and tape writing;
- pattern recognition on a sample of events (see subsection 5.2.4.2);
- filling of various histograms (see subsection 5.2.4) and tables for monitoring purposes.

5.2.3 Dead-time

The acquisition of an event is done in three steps, each one being a possible source of dead-time:

i) Transfer from the RMH to an event-buffer. After strobing into the RMH memory, the data are transferred to the first free event-buffer. The transfer time depends on the multiplicity and on the topology of the event: channels in a given receiver module are transferred at a higher speed than channels in different modules located in different crates. Typical times are 100 to 200 ns per address. An event is rejected if its length exceeds a given size, which is preset in the RMH interface of the event-buffer. The maximum is 2048 words, i.e. the actual size of the memory.

ii) Processing of the data by GESPRO. This is done in parallel with the acquisition of a successive event and/or the transfer of a preceding one to the on-line computer. In normal running conditions, one of the four GESPROs is almost always idle, three of them being sufficient for the processing. The dead-time due to GESPRO is therefore almost negligible.

iii) Transfer from the event-buffer to the on-line computer. This transfer rate is limited by the CAMAC cycle, which is about 3 μs per 16-bit word.

Under normal running conditions, the total dead-time is less than 4%.

5.2.4 On-line monitoring

The architecture of the on-line computer allows several monitoring jobs to be run in the ND 100 without slowing down the processing executed by the ND 500. This increases the monitoring power of the system without reducing its efficiency.

The monitoring power is further improved by the fact that all the trigger configurations are fully programmable. The trigger logic can therefore be rapidly checked without any recabling.

All the elements of the spectrometer, as well as the data-taking and the beam line, are permanently monitored.

It is worth emphasizing here that all histograms described below are incremented event-by-event.

5.2.4.1 Hodoscopes and trigger logic

A histogram ("Counter Illumination"), with bins representing each counter and channel of the trigger logic, is provided to pin-point anomalies such as dead counters, channels permanently firing, etc.

All photomultiplier voltages are checked at 15-minute intervals.

5.2.4.2 MWPCs

To each active wire there corresponds one bin in the "Chamber Illumination" histogram. Its purpose is to locate dead channels. A valuable check of the operation of the MWPCs is the on-line determination of their efficiencies. This is done as follows:

i) Segments of muon tracks are searched for in the downstream chambers; this search is first done in the three projections and thereafter by associating them to form a track.

ii) Segments in the upstream chambers are searched for, requiring that the hits be in a "road" around the line connecting the target to the intersection of the tracks from step (i) with the virtual bending plane.

iii) A complete muon track is then defined as a pair of segments, one upstream and one downstream, meeting at the virtual bending plane.

iv) The number of missing hits determines the inefficiency of the chambers (see fig. 4).

This pattern recognition is performed on events smaller than 750 words. The reliability of the method was checked by making a comparison with chamber efficiencies computed off-line.

The on-line computation of the chamber efficiencies allows the delay curves and the plateaus of the chambers to be measured in a quick and accurate way during the setting-up of the apparatus.

Additional parameters, such as cluster sizes, hit multiplicities, and the occurrence of holes between fired wires ("eyes"), are also available.

5.2.4.3 Quality of the events

The event quality is monitored by histogramming a number of parameters, e.g.

- over-all event size;
- number of hits in the chambers;
- dimuon mass (as computed by GESPRO);
- time of arrival of the event in the burst (this reflects the structure of the beam spill);

In addition, it is verified that the RMH addresses are in strictly increasing order; errors are recorded.

5.2.4.4 Event-buffer/microprocessor system

If something is hung-up in the transfer from RMH to buffer or from buffer to computer, the operation is interrupted by a time-out, whose value can be set by program. Transfer errors and other sources of trouble are checked and recorded by the ND 100/500.

5.2.4.5 Magnetic field

Two parameters related to the field are recorded burst-by-burst: the magnet current, and the voltage of a Hall probe mounted at a reference point.

5.2.4.6 Beam line

The values of the main beam monitors are histogrammed burst-by-burst and their deviations from the mean values are computed and checked continuously. The mean values for each run are stored on disk and are available for checking the stability.

5.2.4.7 Data-taking

The main potential source of errors is a possible lack of response to BOB and EOB interrupts and to the LAM generated by the DMA interface. Such errors are corrected by imposing software time-outs, whose occurrence is monitored.

The loss of synchronization between BOB and EOB (e.g. two following BOBs without an intermediate EOB) is considered a "fatal error"; such errors stop the data-taking.

6. OFF-LINE PROCESSING

6.1 Organization of the data-processing

The raw data tapes, written by the ND 100/500 in standard format [9], contain, for each event, the information from the RMH and from GESPRO, and, for each burst, the contents of the scalers and the information on the beam transport elements. These tapes are processed by a general-purpose program, which performs the event reconstruction and filtering and writes the reconstructed events on tape. In addition to the raw data, all information on the reconstruction is saved.

In a second step, dimuon events with masses above 4 GeV/c^2 are selected and written on data summary tapes (DST). A further selection is made to get rid of most of the background (spurious) events; the kinematics of the surviving events is written on a micro-DST. All the information relevant for the analysis is thus found on a single tape.

All the parameters corresponding to a given geometrical configuration are kept in a file which can be accessed by all programs.

6.2 Reconstruction program

This program contains not only the reconstruction routines but also a series of routines which check the alignment of the detectors and compute the efficiencies of the chambers, of the hodoscopes, and of the trigger electronics.

6.2.1 Pattern recognition

Once the RMH information is decoded, the configuration of the counter hits is compared with the trigger logic. Only 0.3% of the triggers have an inconsistent configuration and are rejected.

The pattern recognition uses a modified version of a known algorithm (PTRACK1 [10]): straight tracks are searched for in the three projections corresponding to the three wire orientations. At least three wire hits are required to define a track in one projection. The tracks are then associated in space; the remaining tracks in two different projections are associated if they coincide with two wire hits in the third one. The downstream chambers are investigated first, since the number of wire hits is smaller behind the magnet. The target and the tracks already found in the downstream chambers are used to constrain the search in the upstream chambers.

The tracks found in the two MWPC telescopes are associated on the basis of closeness in the magnet mid-plane and of coplanarity. They are then compared with the hodoscope configuration, and trajectories not validated by counter hits are rejected.

6.2.2 Momentum estimate

In a purely azimuthal field, trajectories can be computed by quadrature. As the integrals cannot be done analytically, a first approximation for the momentum, valid for a small bending angle θ, is obtained by expansion (see subsection 3.3). To get a better estimate, the field is subdivided into several intervals, in such a way that θ in any one interval is less than 0.5 mrad. Summing over all the intervals, a value of θ is obtained and is compared with the measured one; the approximate momentum is then corrected for the difference. If necessary, a further iteration is

made, until this difference becomes negligible. In most cases, one or two iterations are enough, less than 1% of the tracks needing a further one. A fringe-field correction is also applied.

The final momentum accuracy is better than 2%, almost independently of the p_T of the muon. It is limited essentially by the accuracy of the tracking. Momenta are finally corrected for the average energy loss in the hadron absorber and in the target.

6.2.3 Vertex computation

The vertex is defined by the directions of the two muon tracks, as measured beyond the absorber, and by the direction of the incident beam. To allow for the multiple scattering in the hadron absorber, each muon track is given a weight proportional to the square of its momentum. The beam direction is weighted by its r.m.s. lateral spread, 1.6 mm. The vertex is computed as the point of closest approach of these three weighted lines. The vertex distribution along the beam axis is shown in fig. 7: the target is clearly separated from the dump; the FWHM at the target is 48 cm for a 12 cm long tungsten target. As the target length is small compared to the FWHM the vertex is assigned to the target centre.

The multiple scattering of the tracks in the muon filter can be shown to be equivalent to a lateral displacement and to an angular deflection (uncorrelated) in a plane located at the average depth of the filter; the depth is computed taking into account the radiation lengths of the different materials. Thus there are two *independent* estimates of the track direction: one is obtained by joining the vertex to the intersection of the track with the "plane of no correlation"; the other is the measured one. Their weighted average yields the best estimate of the direction of the track at the vertex. Note that this best estimate is readily obtained with the so-called "Magic Plane" [11].

6.2.4 Program efficiency and processing time

The various cuts (wire hits, track association) applied in the reconstruction introduce an estimated event loss of 3.6% at 10^9 π per burst, and of 8% at 2×10^9 π per burst.

The processing time on the CERN CDC 7600 computer is about 36 ms per trigger.

6.3 Simulation program

This Monte Carlo program serves to compute the acceptance and the resolution of the spectrometer, and also to study possible biases of the trigger.

6.3.1 Event generation

The event configuration, for a given dimuon mass and beam momentum, is derived from known distributions: structure functions, dimuon transverse momentum P_T, angular distributions, etc. The Fermi motion of the nucleon [12] and the momentum spread of the beam (see subsection 2.2) are taken into account. The two muons are followed through the apparatus, allowing for effective target length, energy loss (including straggling) by ionization, bremsstrahlung and pair creation, multiple scattering, detector sizes and shapes, dead regions, wire spacing, etc. The tracks are traced through the magnetic field using the algorithm NYSTRK [10] with the same field parametrization as in the reconstruction program. Finally, the trigger conditions are imposed on the events. The simulated events are processed by the same reconstruction program as is used for the real ones.

The simulation program was checked by comparing the distributions of kinematical parameters with those of real events. The computing time per accepted event is about 40 ms on the CDC 7600 computer.

6.3.2 Acceptance

The acceptance of the spectrometer was determined by a Monte Carlo calculation as described above. The result is shown in fig. 8 for 200 GeV/c pions, as a function of the dimuon mass M, of the Feynman variable x_F, and of the dimuon transverse momentum P_T (integrating over all the other variables). The acceptance in x_F allows a good determination of the pion structure function.

6.3.3 Resolution

The resolution of the spectrometer depends mainly on the accuracy of the momenta and of the vertex angles, which is mostly limited by the multiple scattering and energy loss straggling in the hadron absorber. Figure 9 shows the computed mass resolution $\Delta M/M$ as a function of the mass, as well as the muon momentum resolution $\Delta p/p$ and the vertex angle resolution $\Delta\theta/\theta$. The resolutions at the masses of the J/ψ and of the Υ, as obtained from a Gaussian fit to our data, confirm the results of the simulation program.

7. CONCLUSION

The apparatus described here was installed at CERN in 1980. Preliminary data allowed the study of the A-dependence of the dimuon production [13]. All parts of the apparatus, including the data-acquisition system, worked with great reliability over long periods. During 1981 and 1982, some 10 million triggers were recorded and fully reconstructed in the following months.

Data-taking was resumed in 1983 with an incident beam of 300 GeV/c negative pions. In addition to the tungsten target, a 120 cm liquid-hydrogen or deuterium target was installed, and the trigger logic was modified to allow simultaneous exposure of both targets.

Acknowledgements

Many people contributed to the various aspects of our apparatus. Special thanks are due to

- the technical and engineering staff of the collaboration, for the design, construction, and setting-up of the various components of the spectrometer;
- the STIPE (Service des Techniques Instrumentales des Particules Élémentaires, CEN Saclay) for their contribution to chamber design, and for the construction of the four large chambers;
- the Instrumentation Group of the CERN Experimental Facilities Division for their collaboration in the realization of the event-buffer/microprocessor system, and their continued assistance in its maintenance;
- J.P. Melot (Bristol University) for his participation in the design of the event-buffer memory and interface;
- the Magnet Assembly and the Magnet Measurement Groups of the CERN Experimental Physics Division, and the Super Proton Synchrotron (SPS) Survey Group;
- the Experimental Area Group of the SPS for providing the high-intensity pion beam;
- the crew of ECN3 for their work in installing the spectrometer.

In addition, we wish to thank J. Badier and W. Kienzle for their participation in the design of the spectrometer.

REFERENCES

[1] S.D. Drell and T.M. Yan, Phys. Rev. Lett. 25 (1970) 316.

[2] *CERN SPS Experimenters' Handbook*, ed. M. Reinharz, CERN, 1981.

[3] Ch. Iselin, CERN 74–17 (1974).
N. Doble and K. Freudenreich (private communication).

[4] H.W. Atherton *et al.*, CERN 80–07 (1980).

[5] V. Agoritsas, Proc. Particle Accelerator Conference, Washington DC, 1981, ed. R.C. Placious [IEEE Trans. Nucl. Sci. **NS–28** (1981) 2243].

[6] J.B. Lindsay *et al.*, Proc. Wire Chamber Conference, Vienna, 1978, eds. W. Bartl and M. Regler [Nucl. Instrum. Methods **156** (1978) 329].

[7] A. Coc, *Thesis*, Université de Paris VII, 1980 (unpublished).

[8] J.P. Froberger, *Thesis*, CRN/HE 80–11, CRN and Université Louis Pasteur, Strasbourg, 1980 (unpublished).
J. Lecoq, *Thesis*, CRN/HE 83–01, CRN and Université de Haute-Alsace, Mulhouse, 1982 (unpublished).
P. Klein, *Thesis*, CRN/HE 82–05, CRN and Université Louis Pasteur, Strasbourg, 1983 (unpublished).
J. Lecoq *et al.*, CRN/HE 82–04, CRN and Université Louis Pasteur, Strasbourg, 1982.

[9] J. Ogilvie and V. White, CERN DD/OC/80–6 (1980).

[10] *CERN Program Library*, CERN, Geneva, Switzerland.

[11] J.G. Branson, *Thesis*, Princeton University, 1977 (unpublished).

[12] A. Bodek and J.L. Ritchie, Phys. Rev. **D23** (1981) 1070.

[13] S. Falciano *et al.*, Phys. Lett. **104B** (1981) 416.

Table 1
Characteristics of the air core magnet

Over-all length	4800 mm
Over-all outer radius	2050 mm
Magnet acceptance inner radius	295 mm
Magnet acceptance outer radius	1540 mm
Number of turns	32×6
Ohmic resistance	0.06 Ω
Current during bursts	10000 A
Power during bursts	6 MW
Average power (11 s cycle, 2.3 s flat-top)	1.93 MW

Table 2
Selection criteria and rejection factors
($10^9\,\pi$ per burst)

Selection criteria	Rejection	Decision time (μs)
Event buffer memory size	2.7	200
Mass	2.4	38
Total number of words per event	1.6	4
Total number of hits in R hodoscopes	1.2	83
Alignment of V, R3, and R4	1.1	30
Trigger validation by P1 and P2	1.3	4

Figure captions

Fig. 1 NA10 spectrometer.

Fig. 2 MWPC design.

Fig. 3 MWPC plateau and delay curves.

Fig. 4 MWPC efficiencies.

Fig. 5 Fast logic.

Fig. 6 Event-buffer/microprocessor system.

Fig. 7 Vertex distribution for a 12 cm tungsten target.

Fig. 8 Spectrometer acceptance: a) versus dimuon mass M; b) versus Feynman x_F; c) versus transverse momentum P_T.

Fig. 9 Spectrometer resolution, as determined by Monte Carlo (curves) and by a fit to the data (circles).

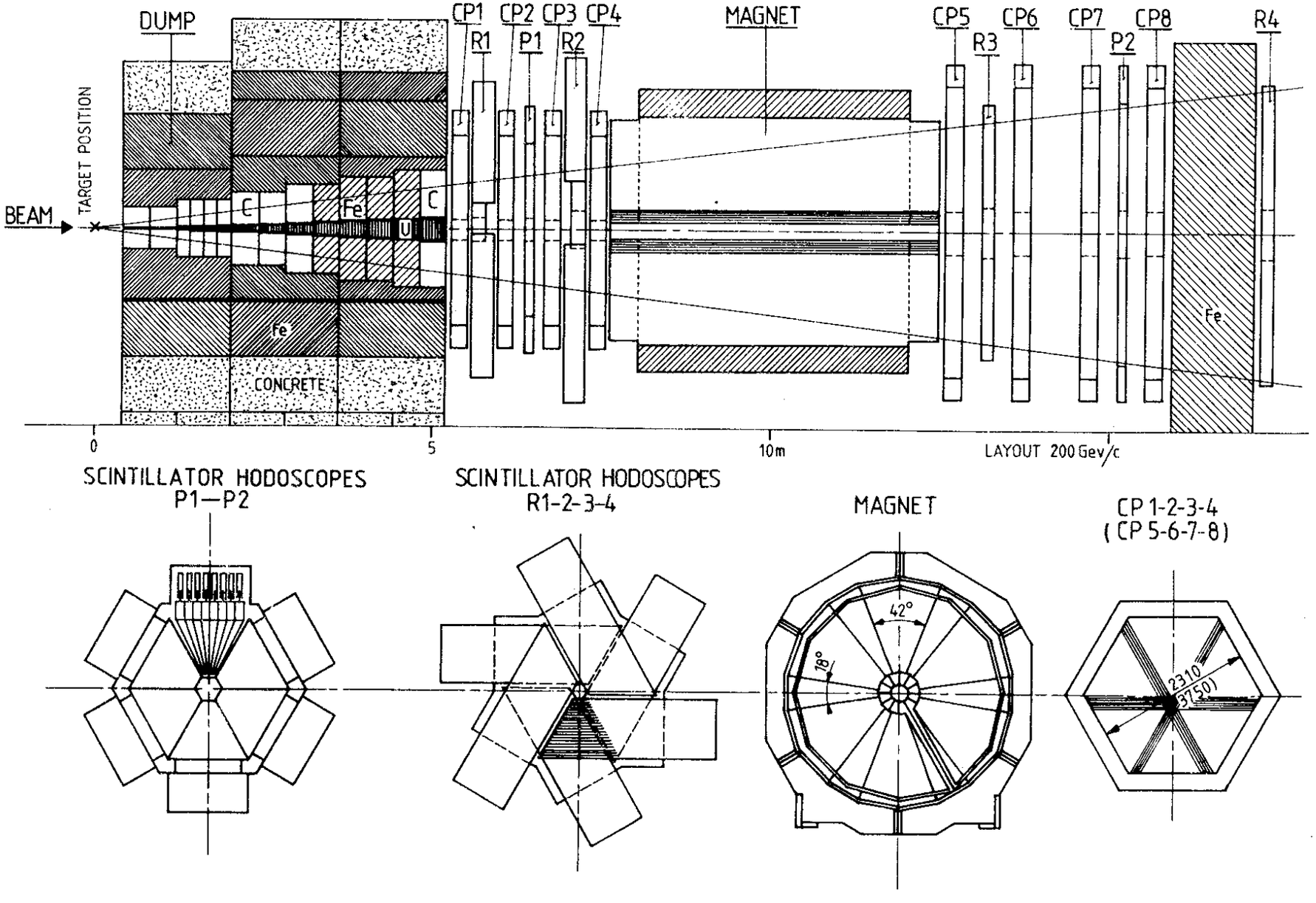
DUMP
CP1
CP2
CP3
CP4
MAGNET
CP5
CP6
CP7
CP8
R4
R1
P1
R2
R3
P2
TARGET POSITION
BEAM
C
Fe
U
C
Fe
CONCRETE
Fe
0
5
10m
LAYOUT 200 Gev/c
SCINTILLATOR HODOSCOPES
P1—P2
SCINTILLATOR HODOSCOPES
R1-2-3-4
MAGNET
42°
18°
CP 1-2-3-4
(CP 5-6-7-8)
2310
3750

Fig. 1

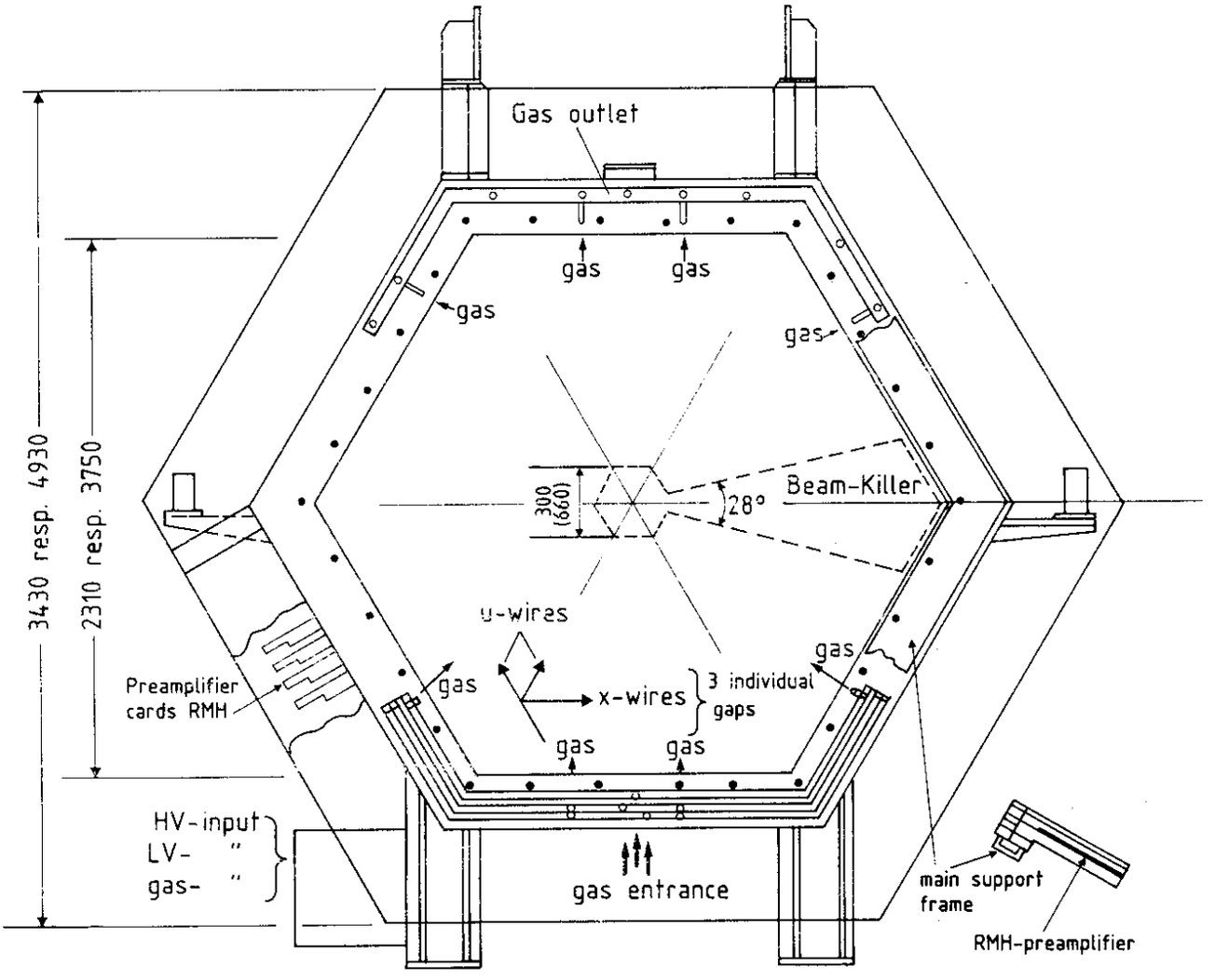

a) Front view of the multiwire proportional chamber

Fig. 2

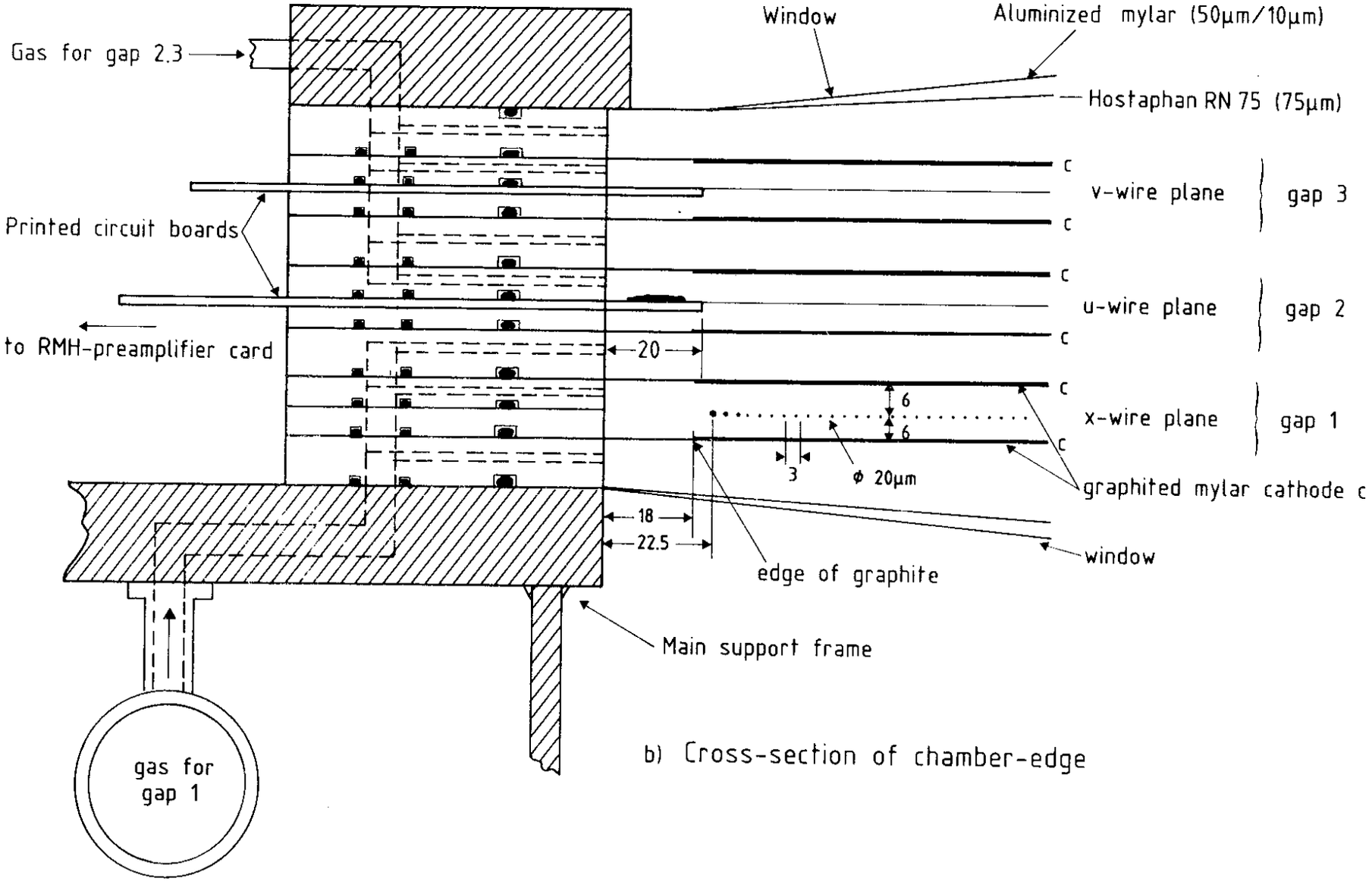

b) Cross-section of chamber-edge

Fig. 2 (contd.)

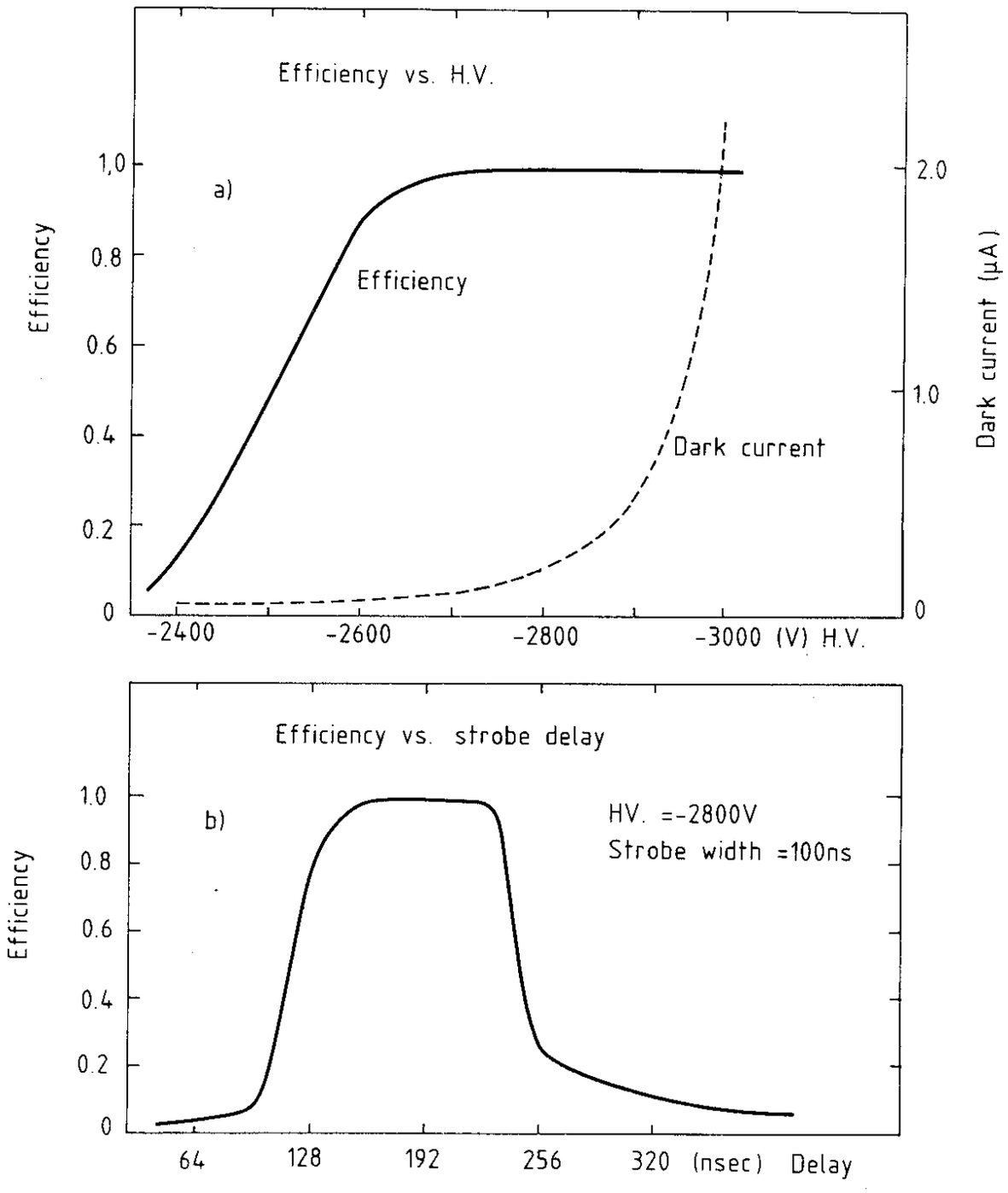
Efficiency vs. H.V.
a)
Efficiency
Dark current
Efficiency
1,0
0.8
0.6
0.4
0.2
0
2.0
1.0
0
Dark current (μA)
-2400
-2600
-2800
-3000 (V) H.V.
Efficiency vs. strobe delay
b)
HV. =-2800V
Strobe width =100ns
Efficiency
1.0
0.8
0.6
0.4
0.2
0
64
128
192
256
320 (nsec) Delay

Fig. 3

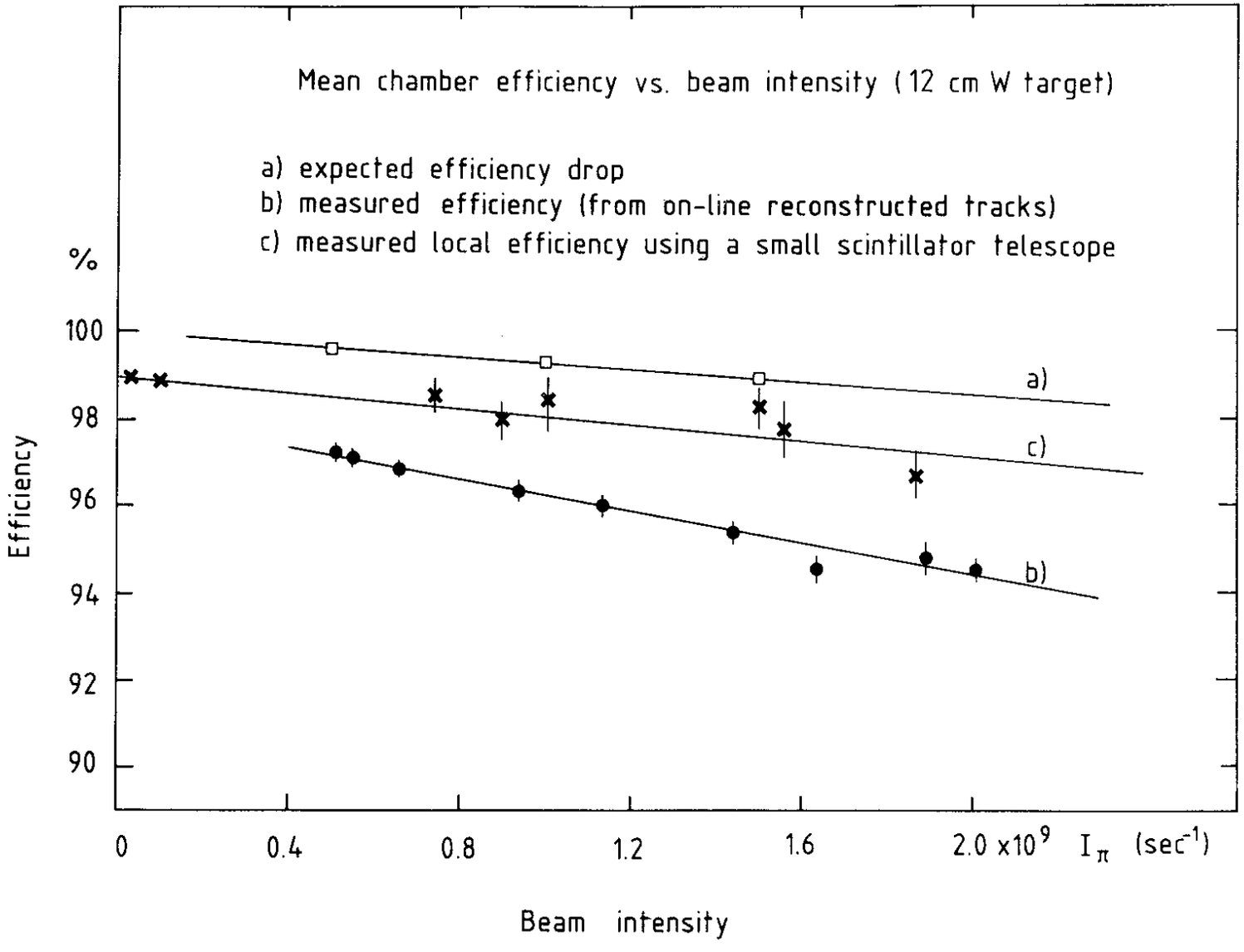
Mean chamber efficiency vs. beam intensity (12 cm W target)
a) expected efficiency drop
b) measured efficiency (from on-line reconstructed tracks)
c) measured local efficiency using a small scintillator telescope
%
100
98
96
94
92
90
Efficiency
a)
c)
b)
0
0.4
0.8
1.2
1.6
2.0 x10^9 I_π (sec^-1)
Beam intensity

Fig. 4

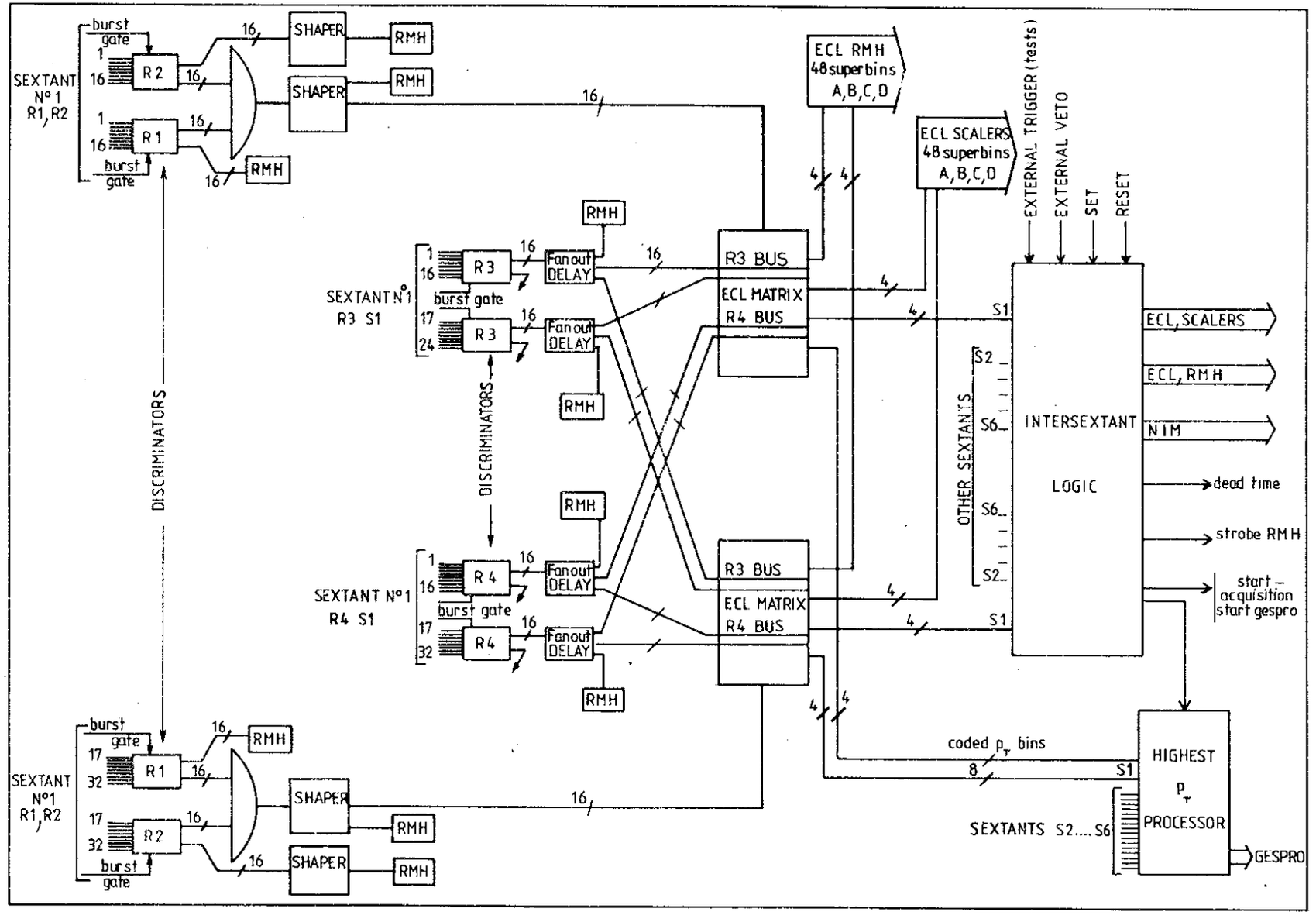
SEXTANT N°1 R1, R2
burst gate
R2
R1
SHAPER
RMH
DISCRIMINATORS
SEXTANT N°1 R3 S1
R3
Fanout DELAY
SEXTANT N°1 R4 S1
R4
R3 BUS
ECL MATRIX R4 BUS
ECL RMH 48 superbins A,B,C,D
ECL SCALERS 48 superbins A,B,C,D
EXTERNAL TRIGGER (tests)
EXTERNAL VETO
SET
RESET
OTHER SEXTANTS
INTERSEXTANT LOGIC
ECL, SCALERS
ECL, RMH
NIM
dead time
strobe RMH
start – acquisition start gespro
coded p_T bins
HIGHEST p_T PROCESSOR
SEXTANTS S2.... S6
GESPRO

Fig. 5

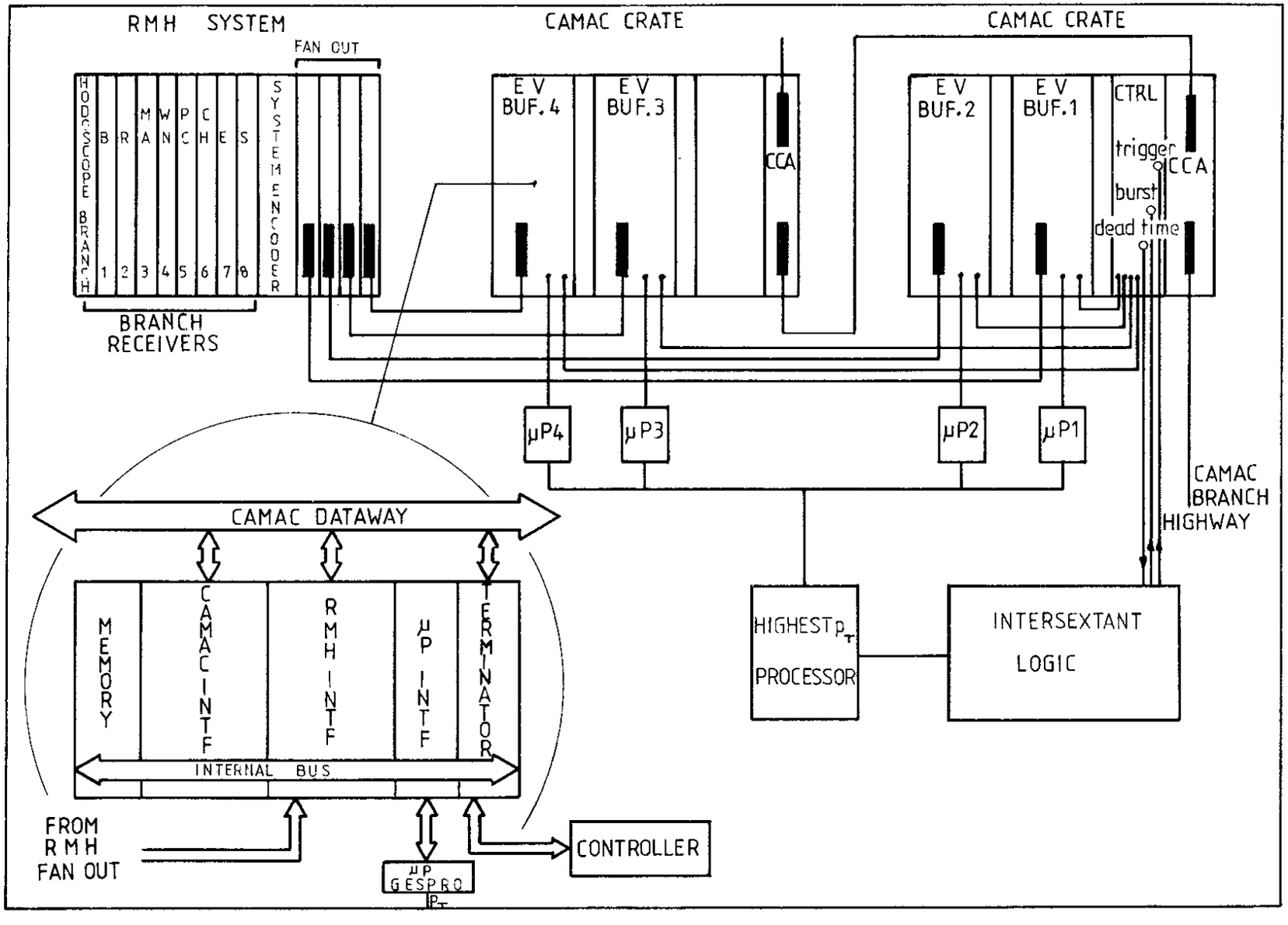
RMH SYSTEM
FAN OUT
HODOSCOPE BRANCH
B R MA WN PC CH ES
1 2 3 4 5 6 7 8
SYSTEM ENCODER
BRANCH RECEIVERS
CAMAC CRATE
EV BUF. 4
EV BUF. 3
CCA
CAMAC CRATE
EV BUF. 2
EV BUF. 1
CTRL
trigger
burst
dead time
CCA
μP4
μP3
μP2
μP1
CAMAC BRANCH HIGHWAY
CAMAC DATAWAY
MEMORY
CAMAC INTF
RMH INTF
μP INTF
TERMINATOR
INTERNAL BUS
HIGHEST p_T PROCESSOR
INTERSEXTANT LOGIC
FROM RMH FAN OUT
μP GESPRO p_T
CONTROLLER

Fig. 6

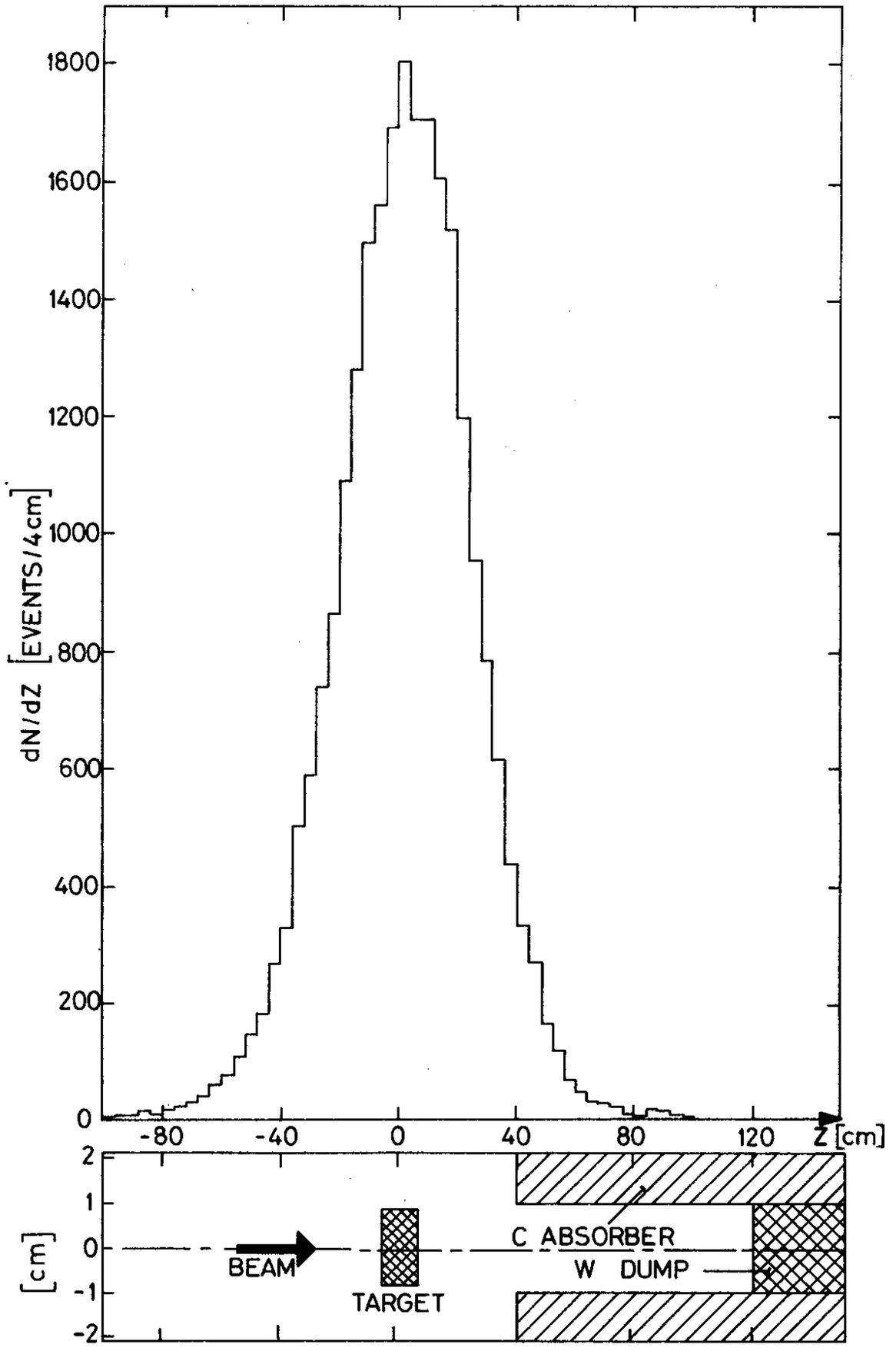
1800
1600
1400
1200
1000
800
600
400
200
0
dN/dZ [EVENTS/4cm]
-80
-40
0
40
80
120
Z [cm]
2
1
0
-1
-2
[cm]
BEAM
TARGET
C ABSORBER
W DUMP

Fig. 7

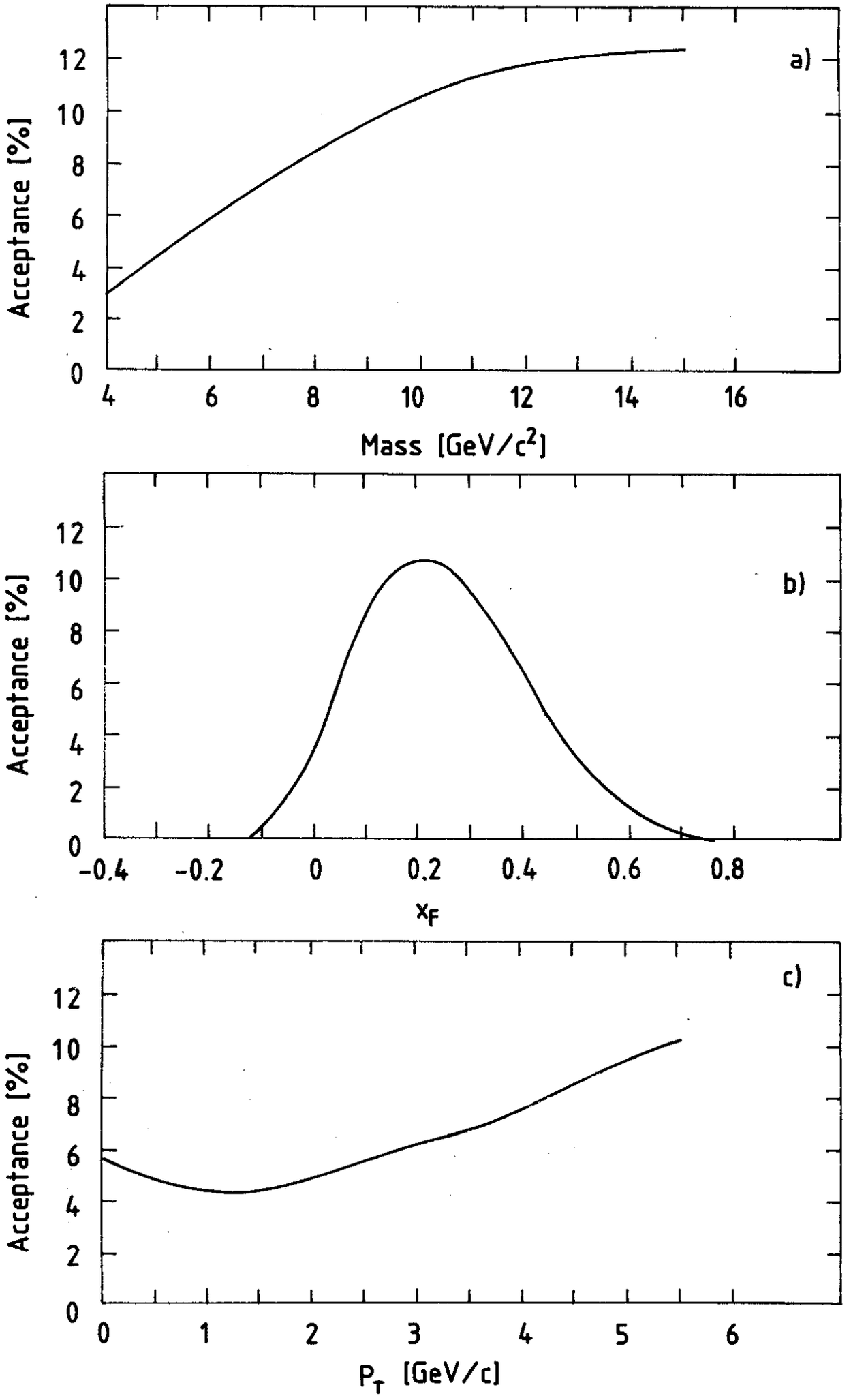
a)
Acceptance [%]
Mass [GeV/c²]
b)
Acceptance [%]
x_F
c)
Acceptance [%]
P_T [GeV/c]

Fig. 8

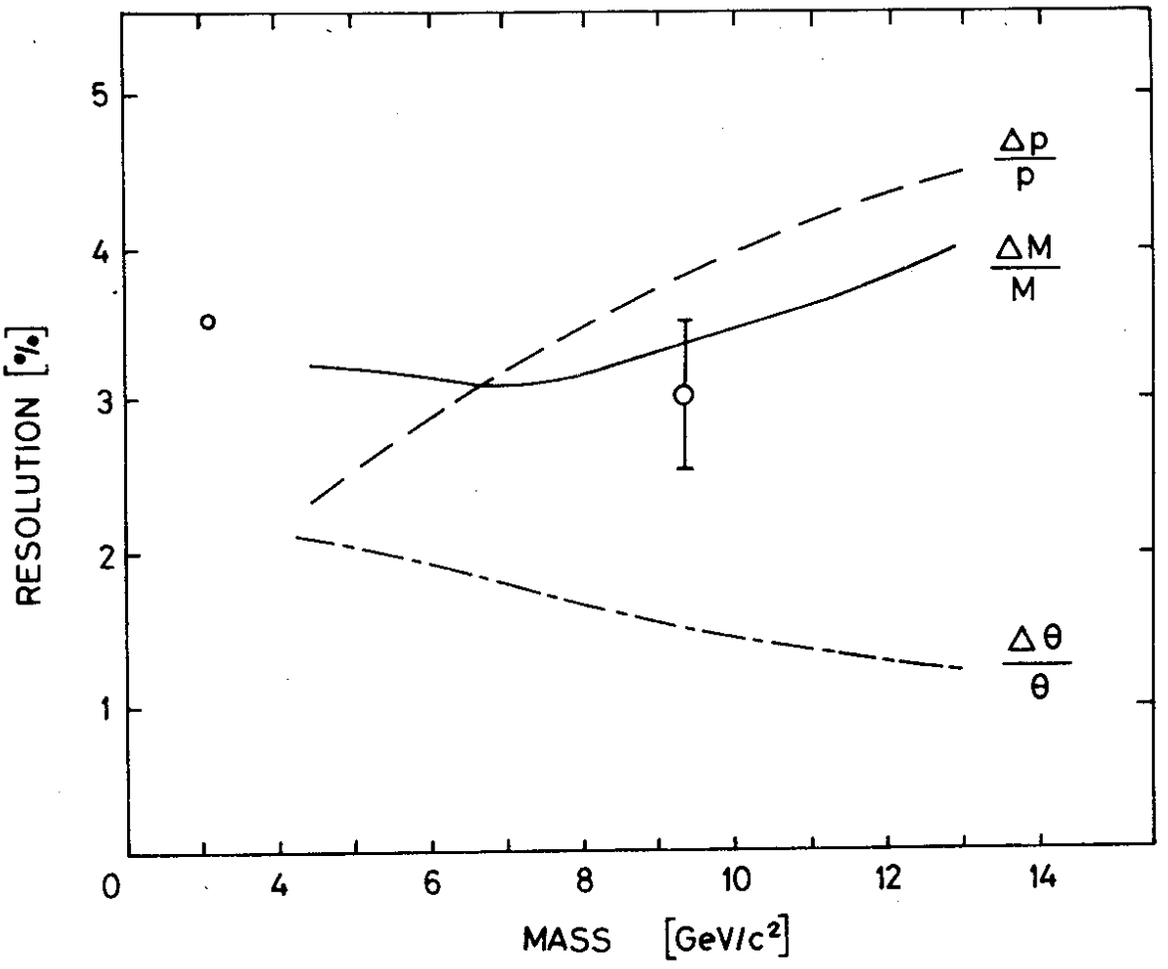

Fig. 9